Platform Alignment Using a Strapdown Stellar Sensor

JEFFREY M. NASH AND GERALD R. WELLS*
Logicon, Inc., San Pedro, Calif.

This paper examines the use of a body-mounted stellar-sighting device to align an aerospace vehicle's gimballed inertial measurement unit. The fundamental observability of not only platform misalignments but also time-invariant sensor-mounting errors is demonstrated. The performance of an inflight estimation algorithm is shown to be a function of several environmental and navigation hardware parameters as well as the characteristics of the sighting device itself. Parametric case studies are presented for a sample system.

Summary

A BODY-mounted stellar-sighting device is used to estimate misalignments in an inertial measurement unit (IMU) of an aerospace vehicle. Assuming that the vehicle's body motion permits sighting on two or more target stars, the analytical feasibility of the approach presented is assured. Results indicate that the most sensitive elements affecting performance in the linkage of stellar sensor-to-platform coordinates are the IMU gimbal angle resolvers. Other relevant parameters include sensor accuracy, star separation, vehicle dynamics, sensor orientation, and modeling errors.

A notable feature of the approach presented is that significant manufacturing tolerance errors, normally incurred in the mounting of strapdown optical devices, can be aligned and corrected by in-flight measurements and computations. Thus, elaborate manufacturing and preflight calibrations are avoided by employing in-flight computation. Such an approach is obviously attractive for vehicles already possessing suitable computational capability.

Introduction

In a variety of space navigation applications, it is frequently desirable to align inertial navigation equipment using stellar sensing devices. Such an approach is particularly attractive whenever prelaunch access to navigation instrumentation is restricted or impossible. One technique for obtaining appropriate calibration is to mount a stellar sensor directly onto an IMU. Although navigation can be improved considerably by a platform-mounted sensor,[1] viewing restrictions, bulkiness, and manufacturing considerations limit the usefulness of such devices. An alternate approach, yielding superior flexibility, is to mount a stellar sensor on the vehicle body itself. However, the ultimate accuracy attributable to using such strapdown devices is generally governed by the accuracy with which the sensor reference frame is known relative to the navigation reference frame. But, for strapdown applications, it will be demonstrated that the use of estimation theory can permit a relaxation of manufacturing tolerance requirements at the expense of in-flight computation.

For the applications examined in this article, it is assumed that the vehicle's IMU is coarsely aligned prior to initiation of the stellar sighting process. The purpose of the stellar sighting is to refine the initial alignment. Both the feasibility and effectiveness of a strapdown sighter mechanization are issues of concern as is the determination of performance-parameter values.

The vehicle configuration chosen for study is shown in Fig. 1. The vehicle is cylindrically shaped and spins about its axis of symmetry; the star sighter is assumed to be rigidly mounted to the base of the vehicle body. The sighter is inclined relative to the vehicle spin axis so that, as the vehicle spins, a cone of view is swept out by the sensor's field of view (FOV). If, in addition to the simple spinning depicted in Fig. 1, the vehicle is prone to coning motion, a more complex system FOV results.

The basic measurement made by the system under study is the direction of the line of sight (LOS) to a star measured relative to the sensor centerline and referenced to inertial space as represented by a stabilized platform. To analytically predict the direction of the LOS of the star relative to nominal coordinate frame orientation, the sighter system software uses the expected orientation of the platform-mounted accelerometers (relative to the IMU gyros), the expected orientation of the IMU case relative to the stellar sensor, and the measured platform gimbal angles. An overview of the system is shown in Fig. 2. The indicated misalignment angles form twelve states in a Kalman filter. Analysis and simulation show that the estimation errors of these misalignment states become successively smaller only if the vehicle is spinning, if two stars can be observed, and if the various constant coordinate transformation misalignments are modeled and estimated in the onboard computer.

The process of estimating misalignments in each of the coordinate transformations relating the stellar sensor to the accelerometer reference frame yields a significant result; mounting the devices in the vehicle need not be performed with extreme accuracy. Studies to date indicate that sighter mounting misalignments can be accommodated with little effect on system

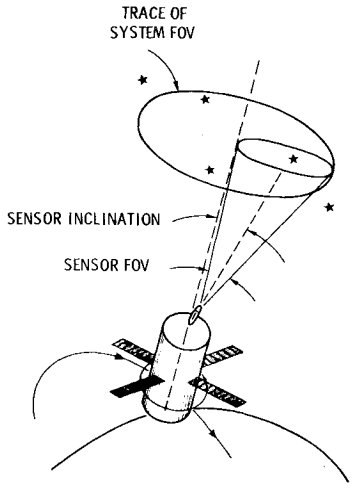

Fig. 1 Sensor system geometry.

Received June 14, 1974; revision received October 21, 1974. This work was funded by USAF Contract F04701-71-C-0161. Appreciation is acknowledged for the valuable contributions and assistance of E. F. Stafford, USAF.

Index categories: Navigation, Control, and Guidance Theory; Spacecraft Navigation, Guidance, and Flight-Path Control Systems.

* Member of the Technical Staff, Systems Analysis Dept., Strategic and Information Systems Division. Member AIAA.

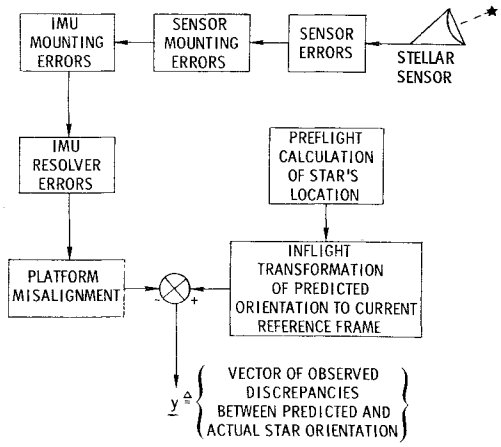

Fig. 2 Stellar calibration block diagram.

accuracy. This result has been verified by analysis, linearized simulation, and nonlinear simulations.

Problem Statement

Figure 2 illustrates that the essential problem requiring mathematical expression is the comparison of measured and predicted values. For this problem the measurements are a star unit vector and the platform gimbal angles. The prediction is based on estimated values of the coordinate transformations linking the star sensor to the IMU, expected values of platform alignment, and the correct values of the star unit vector in inertial space. This heuristic description is formalized below.

The fundamental parameter estimation problem is to estimate a vector of system parameters, $\mathbf{x}(n\times 1)$, given an observation vector, $\mathbf{y}(m\times 1)$, an observation matrix, $H(m\times n)$, and a message or observation model such as

$$\mathbf{y} = H\mathbf{x}+\mathbf{r} \tag{1}$$

The vector $\mathbf{r}(m\times 1)$ is comprised of random noise elements which are assumed to corrupt the observation vector $\mathbf{y}$. The noise vector is assumed to be Gaussian distributed with zero mean and a covariance matrix, $R(m\times m)$. The sequential estimation problem is, simply, to find a best description of $\mathbf{x}$ given repeated values of $\mathbf{y}$, knowledge of the observation matrix H, and statistics of $\mathbf{r}$.

For the stellar sighter problem, $\mathbf{y}$ is taken to be a vector of discrepancies between the vehicle computer's prestored or calculated prediction of a particular star's position relative to the IMU platform and an actual observed position of the same star. The discrepancy between actual and predicted star positions conveys information of system errors, i.e., misalignments.

The state vector, $\mathbf{x}$, is a set of reference misalignments in the system hardware linkages which connect the platform coordinate

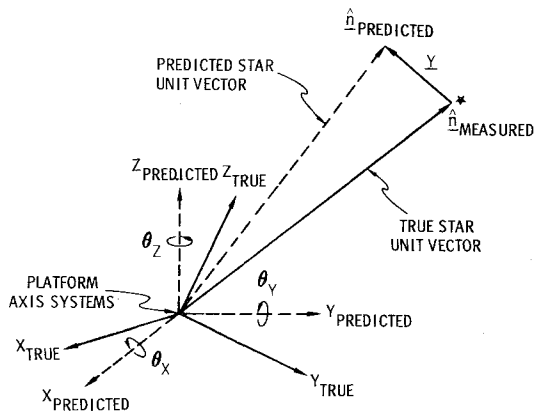

Fig. 3 Stellar observation scheme.

frame with a body-mounted stellar sighter and, ultimately, with the fixed stars. Of principal interest, of course, are the three misalignments (θ_X, θ_Y, θ_Z) which relate the platform's a priori (estimated) alignment to the true alignment, as shown in Fig. 3.

The observation matrix H effectively translates misalignments at various subsystem interface points to observed discrepancy magnitudes in the appropriate frame of reference. Hence, the observation matrix must implicitly contain accurate modeling of essential system dynamics.

The Observation Matrix

For the strapdown stellar sighter under consideration, four transformations and associated error source misalignments are of interest because they affect the ultimate accuracy with which the IMU can be referenced to true inertial space. The transformations and their shorthand representation are as follows:

Stellar sighter to vehicle body:	$[B\leftarrow S]$
Vehicle body to IMU case:	$[C\leftarrow B]$
IMU case to platform:	$[P\leftarrow C]$
Inertial space to platform:	$[P\leftarrow I]$

If it is assumed that there are misalignments between the various hardware system transformation matrices, it is evident that such misalignments will be propagated through a linked system of coordinate transformations which relate sighter coordinate to platform coordinates. Thus, the comparison of the a priori predicted vector of a star in platform coordinates with the a posteriori measured vector (also computed in platform coordinates to platform coordinates. Thus, the comparison of the of intermediate system misalignments including, most significantly, those of the platform relative to true inertial space. The relationship between the misalignments and observed discrepancies is best described in the context of the derivation of the observation matrix H as outlined in the paragraphs which follow.

To obtain an accurate estimation of platform misalignments, it is necessary to express an observed stellar vector discrepancy in terms that account for misalignment inherent to the vehicle navigation reference frame's alignment as well as the stellar sighter's alignment relative to the inertial platform.

Consider the relationship between various system reference frames. The observed discrepancy, $\mathbf{y}$, can be expressed as follows:

$$\mathbf{y} = \hat{\mathbf{n}}_{(\text{predicted})}-\hat{\mathbf{n}}_{(\text{measured})} \tag{2}$$

where $\hat{\mathbf{n}}$ is the platform-to-star unit vector. Expanding Eq. (2) in platform coordinates yields

$$\mathbf{y}_P = [{}_{P_M}\Theta_{P_A}][P\leftarrow I]\hat{\mathbf{n}}_I-\{[P\leftarrow C]+\delta[P\leftarrow C]\}\times [C\leftarrow B][{}_{B_M}\Theta_{B_A}][B\leftarrow S][{}_{S_M}\Theta_{S_A}][S\leftarrow I]\hat{\mathbf{n}}_I \tag{3}$$

where

$$[{}_K\Theta_J] \triangleq \begin{bmatrix} 1 & \theta_Z & -\theta_Y \\ -\theta_Z & 1 & \theta_X \\ \theta_Y & -\theta_X & 1 \end{bmatrix} \triangleq \left\{\begin{array}{l}\text{a unit transformation plus}\\ \text{misalignment error matrix}\\ \text{applicable to measurements}\\ \text{about axes in the}\\ [K\leftarrow J]\text{ transformation}\end{array}\right\} = \{I+[{}_K\varepsilon_J]\}$$

and

$$[{}_K\varepsilon_J] \triangleq \begin{bmatrix} 0 & \theta_Z & -\theta_Y \\ -\theta_Z & 0 & \theta_X \\ \theta_Y & -\theta_X & 0 \end{bmatrix} \triangleq \left\{\begin{array}{l}\text{a small angle misalignment}\\ \text{matrix applicable to error}\\ \text{measurements about axes in}\\ \text{the } [K\leftarrow J]\text{ transformation}\end{array}\right\}$$

and

$$\delta[P\leftarrow C] \triangleq \left\{\begin{array}{l}\text{the error sensitivity of } \mathbf{y} \text{ to gimbal angle}\\ \text{uncertainties. This matrix takes a different}\\ \text{form than } [{}_P\Theta_C] \text{ because the order of rotation}\\ \text{is dictated by the gimbal construction of the}\\ \text{platform, rather than occurring randomly as}\\ \text{would be the case if } [{}_P\Theta_C] \text{ were used.}\end{array}\right\}$$

Expanding Eq. (3) and ignoring terms that are second degree or greater in $[{}_K\Theta_J]$ yields

$$\mathbf{y}_P = \{[{}_{P_M}\varepsilon_{P_A}][P \leftarrow I] - \delta[P \leftarrow C][C \leftarrow I] - [P \leftarrow B][{}_C\varepsilon_B][B \leftarrow I] - [P \leftarrow S][{}_B\varepsilon_S][S \leftarrow I]\}\hat{\mathbf{n}}_I \quad (4)$$

Equation (4) expresses the observable quantity in terms that account for misalignment angles occurring at the indicated subsystem interface points as well as those occurring as a consequence of the platform's misalignment relative to the inertial frame.

It is necessary to assume that each error source acts independently since the misalignments are regarded as random (bias) errors. As an example, consider the first element on the right-hand side of Eq. (4). That is, let

$$\mathbf{y}'_P = [{}_{P_M}\varepsilon_{P_A}][P \leftarrow I]\hat{\mathbf{n}}_I = \begin{bmatrix} 0 & \theta_Z & -\theta_Y \\ -\theta_Z & 0 & \theta_X \\ \theta_Y & -\theta_X & 0 \end{bmatrix} \begin{bmatrix} PI_{11} & PI_{12} & PI_{13} \\ PI_{21} & PI_{22} & PI_{23} \\ PI_{31} & PI_{32} & PI_{33} \end{bmatrix} \begin{bmatrix} n_X \\ n_Y \\ n_Z \end{bmatrix} \quad (5)$$

Treating the θ_X term, for example, yields

$$\mathbf{y}'_{P_X} = \begin{bmatrix} 0 & 0 & 0 \\ 0 & 0 & \theta_X \\ 0 & -\theta_X & 0 \end{bmatrix} [P \leftarrow I]\hat{\mathbf{n}}_I = \begin{bmatrix} 0 \\ PI_{31}n_X + PI_{32}n_Y + PI_{33}n_Z \\ -PI_{21}n_X - PI_{22}n_Y - PI_{23}n_Z \end{bmatrix} \theta_X \quad (6)$$

The previous equation is simplified by making the following definition

$$\mathbf{H}_{0_1} \triangleq \begin{bmatrix} 0 \\ PI_{31}n_X + PI_{32}n_Y + PI_{33}n_Z \\ -PI_{21}n_X - PI_{22}n_Y - PI_{23}n_Z \end{bmatrix}$$

It is recognized that $\mathbf{H}_{0_2}$ and $\mathbf{H}_{0_3}$ can similarly be constructed for θ_Y and θ_Z, respectively. Electing to aggregate the $\mathbf{H}_{0_i}$'s yields

$$\mathbf{y}'_P = \mathbf{y}'_{P_Y} + \mathbf{y}'_{P_Y} + \mathbf{y}'_{P_Z} = [\mathbf{H}_{0_1} \quad \mathbf{H}_{0_2} \quad \mathbf{H}_{0_3}] \begin{bmatrix} \theta_{0_X} \\ \theta_{0_Y} \\ \theta_{0_Z} \end{bmatrix} \triangleq [H_0][\theta_0] \quad (7)$$

Equation (7) expresses stellar-observable sensitivities arising from platform misalignments in terms of a particular platform alignment and star. Similarly, sensitivity matrices H_i may be derived for misalignments of the sighter relative to the vehicle body H_3, for the platform case relative to the body H_2, and for the gimbal angle error components H_1. With Eq. (7) as a guide, however, the stellar observable can conceptually be expressed as

$$\mathbf{y}_P = [H_0 \,|\, H_1 \,|\, H_2 \,|\, H_3] \begin{bmatrix} \theta_0 \\ \hline \theta_1 \\ \hline \theta_2 \\ \hline \theta_3 \end{bmatrix} + \mathbf{r} \quad (8)$$

where

$[H_i]$ is a 3×3 submatrix of observable sensitivities

and

θ_i is a 3×1 vector of roll, pitch, and yaw misalignments occurring at a particular subsystem interface (e.g., θ_0 is the platform misalignment relative to inertial space).

Observability

The concept and significance of observability in parameter estimation problems is indicated by the following definition: Given the message model of Eq. (1), the system is said to be completely observable over the time interval of interest $[t_o, t_f]$ if every state $\mathbf{x}$ can be determined from the knowledge of $\mathbf{y}(t) = H\mathbf{x}$, for a given t_o and $t_f > t_o$.

The observability of a given message model is determined by the rank of the symmetric Gramian matrix defined by:

$$G = \sum_{k=1}^{N} H_k{}^T H_k \quad (9)$$

where H is defined by Eq. (1).

If G is of full rank (i.e., $|G| \neq 0$), the message and estimation system determined by Eq. (1) is completely observable.

The effectiveness of a minimum variance estimation formulation is dependent upon the degree of observability inherent in the message model employed. By means of the following simplified example[1] it can be shown that the stellar-sighting/inertial-platform-misalignment-estimation problem is fundamentally unobservable whenever only one star is sighted but that sightings on two stars can provide complete observability of (only) the platform misalignments.

Let

$$\hat{\mathbf{n}}_{I_1} = \begin{bmatrix} a \\ 0 \\ 0 \end{bmatrix} \qquad \hat{\mathbf{n}}_{I_2} = \begin{bmatrix} 0 \\ 0 \\ b \end{bmatrix}$$

$[P \leftarrow I] \triangleq$ the 3×3 identity matrix

Then

$$H_1 = \begin{bmatrix} 0 & 0 & 0 \\ 0 & 0 & -a \\ 0 & a & 0 \end{bmatrix} \qquad H_1{}^T H_1 = \begin{bmatrix} 0 & 0 & 0 \\ 0 & a^2 & 0 \\ 0 & 0 & a^2 \end{bmatrix}$$

$$H_2 = \begin{bmatrix} 0 & -b & 0 \\ b & 0 & 0 \\ 0 & 0 & 0 \end{bmatrix} \qquad H_2{}^T H_2 = \begin{bmatrix} b^2 & 0 & 0 \\ 0 & b^2 & 0 \\ 0 & 0 & 0 \end{bmatrix}$$

Clearly, after one sighting, the system will fail the observability test of Eq. (9). However, after two sightings on different stars, Eq. (9) yields:

$$G_2 = \begin{bmatrix} b^2 & 0 & 0 \\ 0 & a^2 + b^2 & 0 \\ 0 & 0 & a^2 \end{bmatrix}$$

which is of full rank and satisfies Eq. (9). Thus, whenever two or more stars are sighted, all platform misalignments become observable and may be estimated in the absence of excessive noise.

From repeated evaluations of Eq. (9), using the aggregate H-matrix described in Eq. (8), several important relationships between estimation state variables were identified. First, the body-mounting errors are inseparable; i.e., those constant misalignments resulting from attaching both the IMU and the star sensor to the vehicle body cannot be distinguished. Additionally, results indicated that for any dynamic environment resulting in gimbal angle excursions and sightings conducted on more than one star, platform pitch and roll misalignments could be estimated and distinguished from all other system misalignments about the platform axes. Results indicated that platform yaw misalignment due to the yaw gimbal's innermost location is indistinguishable from any yaw gimbal error. Nonetheless, the combined platform yaw misalignment and yaw gimbal error was separable from any body-associated yaw misalignments.

In summary, the observability study demonstrated the potential capability of the body-mounted-sighter-estimation concept and justified continued exploration of the effects of initial value variations and noise.

Estimation Results

With the linearized observation model of Eq. (1), existing recursive-minimum-variance-estimation techniques were applied directly to obtain an estimate of the platform and stellar system misalignments as well as the second moment (covariance) of the estimate error. The minimum variance filter propagates estimate information in two channels: one for the estimate itself and another for the statistics of the estimate. A detailed derivation of the minimum variance filter for the linear model of Eq. (1) is given elsewhere[2]; the results are stated next.

Given an initial estimate of the misalignment state vector $\hat{\mathbf{x}}_0$ and an initial covariance of $\hat{\mathbf{x}}_0$, P_0, the estimate and its error covariance are propagated according to the following equations

$$\hat{\mathbf{x}}_{k+1} = \hat{\mathbf{x}}_k + K_{k+1}(\mathbf{y}_{k+1} - H_{k+1}\hat{\mathbf{x}}_k) \tag{10}$$

$$P_{k+1} = [I - K_{k+1}H_{k+1}](P_k + Q_k) \tag{11}$$

where

$$K_{k+1} = P_k H_{k+1}^T (R_{k+1} + H_{k+1} P_k H_{k+1}^T)^{-1} \tag{12}$$

$\triangleq$ the optimal gain matrix for the estimation formulation $(n \times m)$, $Q_k \triangleq E[\boldsymbol{\varepsilon}\boldsymbol{\varepsilon}^T]$ where $\boldsymbol{\varepsilon}$ is a vector $(n \times 1)$ of zero mean Gaussian random error components, i.e., $\mathbf{x}_{k+1} = \mathbf{x}_k + \boldsymbol{\varepsilon}$ and $E[\boldsymbol{\varepsilon}] = \mathbf{0}$. $R_k \triangleq$ the observation noise covariance matrix at the kth estimation instant. $E[\mathbf{r}_k \mathbf{r}_k^T] = R_k$ for the zero mean Gaussian vector $\mathbf{r}_k$.

The estimation performance attainable with the algorithm of Eqs. (10–12) correspond favorably with typical minimum-variance estimation results, provided the linearized estimation model is correct. That is, provided that the following constraints are satisfied

1) The subsystem misalignments, $\theta_{X_1} \ldots \theta_{Z_4}$ (12 elements), are small enough that linearity assumptions remain valid, i.e., $\sin\theta \cong \theta$ and $\cos\theta \cong 1$.

2) The observation $\mathbf{y}$ is indeed comprised of the elements modeled; i.e., a modeling omission or error will result in filter divergence, producing inaccurate results and compromising both the filter and its estimation validity.

For the general linearized estimation formulation there are several comprehensive results. It is well known, for example, that observation and state-vector noise place finite limitations on the ultimate accuracy of the estimate. For the stellar sighting problem, observation noise comprises the resolution and electronic noise (translated into terms and units of $\hat{\mathbf{n}}_I$); state noise represents random uncertainties induced by such factors as gimbal angle resolvers and imposed upon state elements, such as the gimbal angle uncertainty.

Thus, the stellar estimation model explicitly accounts for two types of error: a constant, albeit random, a priori uncertainty (such as platform misalignment) as well as a dynamic random error (such as gimbal angle resolver noise). In the sequel, the first type of misalignment uncertainty is referred to as a bias; the second is identified as a random component or noise imposed upon the misalignment bias uncertainty. Significantly, reliance upon a sophisticated platform error model is not made in this paper. Dynamic errors are assumed to be random.

A Sample Case

To demonstrate the capability of the observation formulation given previously, a sample case was constructed and subjected to analysis. The following assumptions were made regarding the vehicle: 1) It possesses an inertially gimballed IMU and requires misalignment estimation from the strapdown sensor; 2) It spins about its axis of symmetry; 3) Its inertial platform possesses an instantaneous misalignment due to initialization and hardware-induced drifts. For the sample case, a set of ground-rule assumptions were postulated to permit compatible comparisons of parametrically variable system constraints and characteristics. The established ground-rules effectively define a baseline against which performance variations can be compared. It is recognized that for different applications, hardware component accuracy may vary significantly due to cost, weight, and mission requirements. The sample case results portray normalized results to achieve broad appeal. In all cases, normalized values are presented for platform alignment error; i.e., the value given represents a current misalignment value divided by the initial misalignment value. Initially, therefore the normalized error is shown to be 1.0 for all cases. Hence, despite appearances, alignment accuracy is not a function of initial misalignment.

A total of twelve error states are modeled in the baseline system: three platform alignment errors, three gimbal angle resolver errors, three IMU-to-vehicle mounting errors, and three sensor-to-vehicle mounting errors. The vehicle is assumed to be capable of sighting, alternately, on a star located along the X platform axis and another star located 5° off the X platform axis. (Subsequent analysis demonstrated further improvement could be realized from somewhat greater star separation angles.) For brevity, only the estimated platform alignment errors are considered to be criteria in the graphs subsequently presented. Each graph presents the normalized alignment error as a function of parametric variations.

For the sample case, the following assumptions were made: 1) The platform alignment errors are an order of magnitude greater than the resolver or body-mounting errors prior to the initiation of star sighting. For those normalized error results which vary with resolver accuracy, relative error magnitudes suffice to define estimation performance characteristics; 2) The vehicle platform is gimballed from outer to inner in the order of roll, pitch, and yaw; 3) The platform roll gimbal axis is constructed parallel to the body roll axis; 4) The sensor has a standard error of 0.01°, which is well within the state-of-the-art of such devices.[3]

Several environmental and system factors have been shown to have significant influence on the ability of the estimator to accurately determine the vehicle's platform misalignment angles. Among the classes of significant factors are vehicle dynamics-induced effects, star location, and hardware. Each of the error classes will be considered.

The general motion of the axially symmetric, homogenous, cylindrical body is known to be a combination of spinning about the body roll axis coupled with coning about the body angular momentum vector.[4] Given a constant set of mass properties, the vehicle's steady-state motion during free flight is entirely governed by the initial rates imparted to it. For comparison, it is convenient to express the vehicle's initial conditions in terms of steady-state coning (half) angle and spin rate.

The principal interest in vehicle body motion, independently of platform dynamics, which were not addressed, is the time-varying case-to-platform transformation matrix. It is the relative motion between the case and body that produces observability of platform misalignment angles. Generally, it might be anticipated that the greater the gimbal angle excursions imposed by vehicle coning, the greater the resultant observability obtained from the calibration system. Nonetheless, Fig. 4 indicates that maximum and minimum expected coning angle values, differing by an order of magnitude, did not significantly alter the platform calibration performance of the baseline system. The dominant motion that enhances alignment observability is vehicle spin.

The spinning motion of the vehicle permits separation of body-mounting alignment errors from platform initial-misalignment errors by allowing sightings to be made at many different angular positions. The magnitude of coning motion does not significantly improve the attainment of sightings at many different inertial-to-body rotation angles; it merely alters the magnitude of gimbal angles. The absence of spinning motion, however, would not permit separation of body-mounting errors and platform misalignments. Under conditions of strapdown-system sightings conducted in the absence of spinning motion, the results of this study would be significantly altered. In

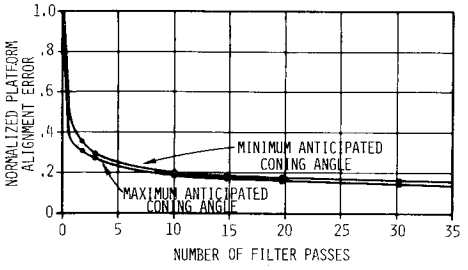

Fig. 4 Effects of vehicle dynamics.

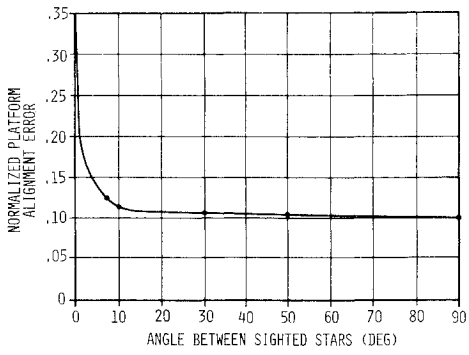

Fig. 5 Effects of star separation after six filter passes.

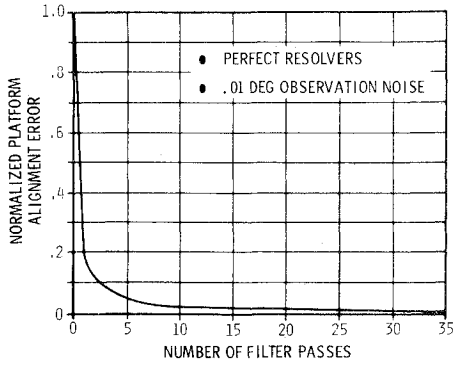

Fig. 7 Limiting accuracy attainable.

particular, alignment calibration could be obtained only if body-mounting errors were minimized.

Another environment parameter that has a significant effect on the calibration effectiveness of the concept under study is the angular separation between the sighted stars. Figure 5 depicts the alignment improvement obtained after six filter passes at various star separation angles. Figure 5 infers that there is a stellar sighting system signal-to-noise threshold; whenever the measurement calibration signal magnitude (as measured by the star separation angle) exceeds the angular resolution noise inherent in the sighter system, nearly optimum performance occurs in terms of limiting values and convergence rate.

It is concluded that no significant benefits were obtained by deliberately increasing the star separation angle in the baseline case. The operational impact of this observation is that star separation constraints do not impose significant bounds on the estimation performance of the baseline system.

Perhaps the most significant class of system errors considered is that comprising initialization and hardware effects. Among the most prominent suspected sources of baseline system accuracy degradation were gimbal angle resolver errors, stellar sighter resolution, sighter mounting errors, and modeling inadequacies.

It is not surprising that the gimbal angle resolvers have a significant effect on the estimation performance of the strapdown concept. The angular transformation that relates stellar observations made in sensor coordinates to predictions and computations in platform coordinates is made through the IMU gimbal angle resolvers. Since the gimbal angles are very dynamic, errors inherent in the resolvers are not only difficult to estimate, but also are extremely detrimental to the alignment calibration process.

Another more obvious factor affecting the calibration capability of the strapdown concept is the accuracy inherent in the electro-optical sensor itself. Clearly, the noisier the observation and its associated error covariance, the more degraded the alignment calibration.

Figure 6 depicts the effects of variation among several random errors. The four graphs presented show the alignment accuracy obtained over two orders of magnitude of potential sensor accuracy for gimbal angle resolvers of various quality. Curves

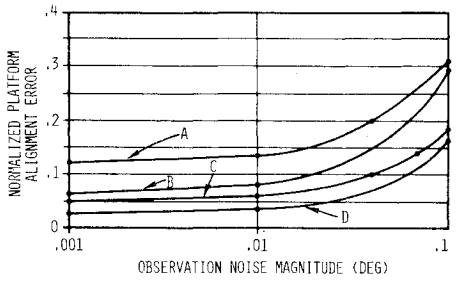

Fig. 6 Effects of random errors after six filter passes.

A and B depict performance after 6 filter passes; curves C and D are for 36 passes. All four curves were generated under the assumption that the gimbal angle resolvers contained a random- and bias-uncertainty component. Curves A and C depict the effect of twice the resolver degradation assumed by curves B and D.

Although the advantage of accurate resolvers is obvious at all values of observation noise, the advantage is greatest at the smaller values for a fixed number of filter passes. Hence, the need for a systems approach is apparent in the design of the strapdown calibration system; resolvers and a stellar sensor must be chosen to complement each other to avoid a costly waste of capability. Similarly, the stellar sensor's accuracy should not be overspecified in an attempt to gain a significant improvement in system performance. A typical relationship is presented in Fig. 6; nearly optimum performance is achieved over a wide range of values for the sample case. Particular hardware characteristics will affect the scale of the curves in Fig. 6, but their shape is invariant.

Figure 7 presents the ultimate attainable performance of the baseline system with perfect resolvers and observation noise corresponding to 0.01°. Convergence is both rapid and asymptotic to within the accuracy of the stellar sensor.

Another hardware-related error source that affects the estimation of platform misalignments is the misalignment between the stellar sighter and the vehicle body itself. Such mounting-error misalignments are attributed principally to manufacturing tolerances and are assumed to be constant once they are incurred.

The specification of such tolerances is indeed significant since it defines the effort required to mate the sensor and vehicle during manufacturing. However, from the observability discussion presented earlier and from computer simulations, it is apparent that the observability of the sensor-to-vehicle and IMU case-to-vehicle mounting errors permits their complete calibration. That is, provided that the assumptions of misalignment-angle linearity ($\sin\theta \cong \theta$ and $\cos\theta \cong 1$) and vehicle motion remain valid, body-mounting errors may be allowed to assume any value. However, note that a more accurately aligned sensor and IMU will result in a somewhat more rapid estimation convergence.

In an effort to determine the necessary dimensions of the estimation state vector and the effects of inaccurate input data, several computational studies were conducted. In particular, it was desired to ascertain what difficulties might be encountered if the body-mounting errors were simply not considered in the estimation formulation. The investigation was motivated by results that demonstrated the relative insensitivity of calibrated alignment to the magnitude of body-mounting misalignment error. Since input accuracy was shown to be relatively independent of body-mounting misalignment errors, it might seem that the body-mounting error contribution to the observed discrepancy need not be explicitly accounted for in the estimation state vector. Such is not the case, however. Filter divergence is experienced whenever significant body-mounting errors exist but

are not modeled. Thus, there is a strong need for adequate modeling.

Conclusions

The technical feasibility of using a strapdown stellar sensor for inflight platform error calibration has been demonstrated. The conceptual method permits a shift of the system accuracy-maintenance burden from pre-flight calibration to in-flight computation. The sample case, although limited in general applicability, demonstrates the potential effectiveness of the concept presented.

References

[1] Nash, J. M., "On the Use of a Simple Stellar Sighter to Determine Booster Navigation Error Parameters," Ph.D. thesis, March 1974, Engineering Systems Department, University of California, Los Angeles, Calif.

[2] Meditch, J. S., *Stochastic Optimal Linear Estimation and Control*, McGraw-Hill, New York, 1969.

[3] Birnbaum, M. M. and Salomon, P. M., "Strapdown Star Tracker for Space Vehicle Attitude Control," *Journal of Spacecraft and Rockets*, Vol. 5, Oct. 1968, pp. 1188–1192.

[4] Goldstein, H., *Classical Mechanics*, Addison-Wesley, Reading, Mass., 1950.

MAY 1975 AIAA JOURNAL VOL. 13, NO. 5

Buckling and Vibration of Cross-Ply Laminated Circular Cylindrical Shells

ROBERT M. JONES* AND HAROLD S. MORGAN†
SMU Institute of Technology, Dallas, Texas

Numerical results from an exact solution are presented for buckling and vibration of simply supported circular cylindrical shells that are laminated unsymmetrically about their middle surface. The coupling between bending and extension induced by the lamination asymmetry substantially decreases buckling loads and vibration frequencies for common composite materials such as boron/epoxy and graphite/epoxy. For antisymmetric laminates, the effect of the coupling dies out rapidly as the number of layers is increased. However, for generally unsymmetric laminates, the effect of coupling dies out very slowly as the number of layers is increased. That is, having a large number of layers is no guarantee that coupling will not seriously degrade the shell buckling resistance and vibration frequencies. Thus, coupling between bending and extension must be included in all analyses of unsymmetrically laminated shells.

Nomenclature

A_{ij}, B_{ij}, D_{ij} = extensional, coupling, and bending stiffnesses of a laminated shell
E_1 = Young's modulus in the 1-direction of a lamina
E_2 = Young's modulus in the 2-direction of a lamina
G_{12} = shearing modulus in the 1–2 plane of a lamina
k_x = normalized axial compression, Eq. (7)
k_y = normalized lateral pressure, Eq. (13)
k_ω = normalized vibration frequency, Eq. (15)
L = shell length (Fig. 1)
m = number of buckle or vibration halfwaves in the x-direction
NL = number of layers in a laminated shell
$\bar{N}_x, \bar{N}_y$ = applied in-surface forces in the x- and y-directions, respectively
n = number of buckle or vibration halfwaves in the y-direction
r = shell radius to the middle surface (Fig. 1)
t = total laminate thickness (Fig. 1)
Z = modified Batdorf shell curvature parameter, Eq. (9)
x, y, z = shell coordinates (Fig. 1)
ν_{12} = Poisson's ratio for contraction (expansion) in the 2-direction due to tension (compression) in the 1-direction

Presented as Paper 74-33 at the 12th AIAA Aerospace Sciences Meeting, Washington, D. C., January 30–February 1, 1974; submitted January 30, 1974; revision received September 20, 1974. This work was partially supported by the Air Force Office of Scientific Research/NA, Air Force Systems Command, USAF, under AFOSR Grant 73-2532.

Index categories: Structural Composite Materials (Including Coatings); Structural Stability Analysis; Structural Dynamic Analysis.

* Associate Professor of Solid Mechanics. Associate Fellow AIAA.
† Research Assistant.

Introduction

CROSS-PLY laminated circular cylindrical shells as in Fig. 1 are common structural elements in the aerospace industry. The advent of advanced fiber-reinforced composite materials such as boron/epoxy and graphite/epoxy with their high potential weight savings has resulted in a significant increase in the use of cross-ply laminated fiber-reinforced shells. Therefore, general knowledge of their vibration frequencies and resistance to buckling is essential. Furthermore, knowledge of their behavior sheds light on the behavior of more complicated laminates such as angle-plys and laminates with mixed orientations.

An important step in learning how to properly laminate shells is to understand the influence of lamination asymmetries about the shell middle surface. Those asymmetries cause coupling

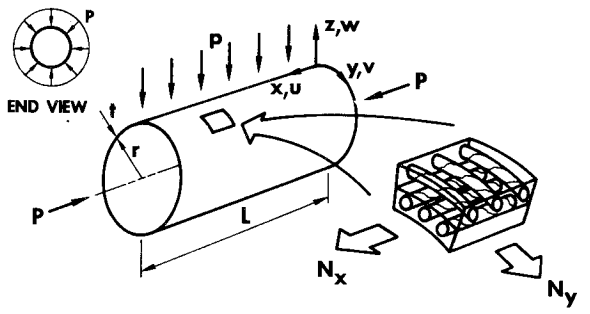

Fig. 1 Laminated shell geometry and loading.